**Proceedings of the ASME 2010 3rd Joint US-European Fluids Engineering Summer Meeting and 8th International Conference on Nanochannels, Microchannels, and Minichannels
FEDSM-ICNMM2010
August 1-5, 2010, Montreal, Canada**

FEDSM-ICNMM2010-30082

ON THE FEASIBILITY OF USING LINEAR FLUID DYNAMICS IN AN OVERALL NONLINEAR MODEL FOR THE DYNAMICS OF CANTILEVERED CYLINDERS IN AXIAL FLOW

M. Kheiri
Department of Mechanical Engineering
McGill University
Montréal, Québec, Canada H3A 2K6

M. P. Païdoussis
Department of Mechanical Engineering
McGill University
Montréal, Québec, Canada H3A 2K6

M. Amabili
Department of Mechanical Engineering
McGill University
Montréal, Québec, Canada H3A 2K6

ABSTRACT

A curiosity-driven study is presented here which introduces and tests an analytical model to be employed for describing the dynamics of cantilevered cylinders in axial flow. This model is called "hybrid" because it encompasses linear fluid dynamics and nonlinear structural dynamics. Also, both the linear and fully nonlinear models are recalled here. For all these models Galerkin's method is used to discretize the nondimensional equation of motion. For the hybrid and nonlinear models a numerical method based on Houbolt's Finite Difference Method (FDM) is used to solve the discretized equations, as well as AUTO, which is a software used to solve continuation and bifurcation problems for differential equations. The capability of the hybrid model to predict the dynamical behaviour of cantilevered cylinders in axial flow is assessed by examining three different sets of parameters. Here, the main focus is put on the onset of instabilities and the amplitude of the predicted motion. According to the results given in the form of bifurcation diagrams and several tabulated numerical values, the hybrid model is proved to be unacceptable although it can predict the onset of first instability, and even the onset of post-divergence instability in some cases.

1. INTRODUCTION

Interest in the vibration of cylindrical structures in axial flow, unlike vibrations of cylindrical structures due to cross-flow, has begun in earnest in the 1950s [1]. Understanding and prediction of the dynamics of cylinders in axial flow is of interest and importance for the design and safe operation of heat-exchanger tubes, nuclear power plants (nuclear fuel bundles, control rods and monitoring tubes), towed flexible cylinders for fresh water and petroleum transportation, towed acoustic streamer arrays for oil and gas exploration, and high-speed trains. Therefore, a considerable number of studies including analytical, numerical and experimental work have been done to examine different aspects of their dynamics.

Historically, the first specific study was made by Hawthorne [2], in which the dynamics and stability of a towed sausage-like flexible body, the Dracone, was investigated. The Dracone was designed and used to transport by sea different lighter-than-sea-water liquids such as petrol, diesel oils, or fresh water to arid lands. Hawthorne proposed the first basic model for the dynamics of such systems.

Later, Païdoussis [3, 4] extended and generalized Hawthorne's work for cylinders with any boundary conditions, e.g., cantilevered or simply-supported, and did some experiments to validate the theory. A more general theory to take gravity and pressurization effects into account, and to deal with cases of confined flow was also developed [5, 6]. In these later studies an error in the equation of motion due to inconsistent incorporation of the viscous forces was corrected; unfortunately, some work, e.g. by Ortloff and Ives [7] and Pao [8], was done in the mean time, based on the erroneous equation of motion.

The divergence (buckling) critical flow velocity for a cylinder with pinned-free boundary conditions was determined analytically by Triantafyllou and Chryssostomidis [9]. The same researchers [10] also studied the dynamics of long, very slender cylinders which were modelled as strings rather than beams. It is noted that, in all the theoretical studies reviewed so far, linear models were used.

The dynamics of cantilevered flexible cylinders in axial flow was later re-examined via a nonlinear theory [11-13]; in this three-part study, (i) the physical dynamics of the system including the experimental observations and the mechanisms of energy transfer, (ii) the derivation of the nonlinear equation of motion, and (iii) the nonlinear dynamics of cantilevered cylinders in axial flow were discussed in detail. Recently, a nonlinear model was developed by Modarres-Sadeghi et al. [14] for flexible cylinders with both ends supported and subjected to axial flow, accounting for the extensibility of the centreline of the cylinder; this was pursued in Ref. [15].

Also, the dynamics of towed cylinders is of interest, not only for their early applications, e.g. the Dracone used for transporting the lighter-than-sea-water products, but also for their recent applications as “seismic arrays” or “acoustic streamers” used for exploring under-sea oil and gas deposits. Over the years theories and models for towed cylinder have been developed alongside the studies made on the other systems, such as cantilevered cylinders in axial flow. Apart the early work done by Hawthorne, several studies on towed systems were made by Païdoussis [16, 17], Pao [8], Païdoussis and Yu [18], Dowling [19, 20], and many others. For a more complete review of this topic, the interested reader is referred to Ref. [1].

More recently, Wang and Ni [21] have reviewed selectively the studies and researches undertaken on vibration of slender structures subjected to axial flow or towed axially in quiescent fluid.

In all experiments to-date, the observed dynamical behaviour of cantilevered cylinders in axial flow is not confined to a plane but it is three-dimensional (3-D); yet no 3-D theory exists to account for that. Therefore, it was considered desirable to extend the existing 2-D analytical model (planar motions) to a 3-D one. However, some aspects of this task proved to be surprisingly difficult, and it was thought worth exploring the capabilities of a simpler model in which linear fluid dynamics would be used while retaining a nonlinear formulation for the structural dynamics. This approach proved very successful for treating the nonlinear dynamics of cylindrical shells conveying fluid [22]. The feasibility of this idea can at present be tested for planar, 2-D motions only.

The rest of present paper is organized as follows: first, some general assumptions and definitions are given, and then the formulation for a fully linear model is recalled. In section 2.3, the nondimensional form of fully nonlinear equation of motion is given according to the formulation in Ref. [12]. The final governing equation for the hybrid model is presented in section 2.4. Then, methods for analysis and solution are discussed briefly. Section 3 is devoted to numerical results and discussion.

2. ANALYTICAL MODELS AND THE SOLUTION METHOD

2.1 General definitions and preliminaries

A flexible cylindrical beam of length L and circular cross-section is considered to be immersed in an incompressible fluid of density ρ, flowing with uniform velocity U parallel to the x-axis, which coincides with the position of rest of the cylinder axis. Except for a short tapering piece of length ℓ fitted to the free end, the cylinder has the uniform cross-sectional area A, mass per unit length m and flexural rigidity EI. As shown in Figure 1, the cylinder is considered to be fixed at the upstream end and free at the other. The motions are supposed to be confined in either a horizontal or a vertical plane, the (x, y)-plane.

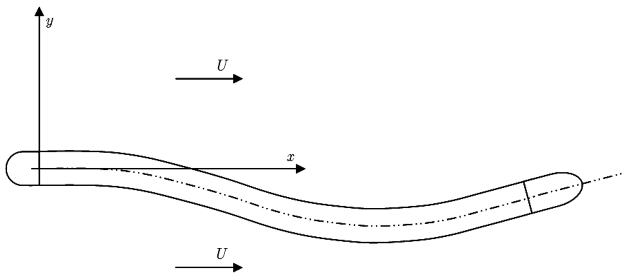

Figure 1. A cantilevered cylinder in axial flow

Only small lateral motions of the cylinder about its position of rest are considered, during which the incidence angle i and $\partial i / \partial x$ remain reasonably small so that (i) no separation occurs in cross-flow and (ii) the fluid forces on each element of the cylinder may be assumed to be identical to those acting on the corresponding element of a long straight cylinder with the same cross-sectional area and inclination.

2.2 Linear model

The linear equations of motion for flexible cylinders in axial flow were derived by Païdoussis [3], and later again in a more general and corrected form [5, 6]. Small lateral motions of the cylinder in unconfined flow may be described by the following equation:

$$\left(E^*\frac{\partial}{\partial t}+E\right)I\frac{\partial^4 y}{\partial x^4}+\rho A\left(\frac{\partial}{\partial t}+U\frac{\partial}{\partial x}\right)^2 y$$
$$-\left\{\delta\left[\bar{T}+(1-2\nu)(\bar{p}A)\right]+\left[\frac{1}{2}\rho DU^2C_T+(m-\rho A)g\right]\right.$$
$$\left.\left[(1-\frac{1}{2}\delta)L-x\right]+\frac{1}{2}\rho D^2U^2(1-\delta)C_b\right\}\frac{\partial^2 y}{\partial x^2}$$

$$+\frac{1}{2}\rho DUC_N\left(\frac{\partial}{\partial t}+U\frac{\partial}{\partial x}\right)y+\frac{1}{2}\rho DC_D\frac{\partial y}{\partial t}$$
$$+(m-\rho A)g\frac{\partial y}{\partial x}+m\frac{\partial^2 y}{\partial t^2}=0, \tag{1}$$

where y is the lateral deflection, C_N and C_T are normal and tangential friction coefficients, respectively, C_b is the base drag coefficient, C_D is the friction drag coefficient, E^* is the viscoelastic constant, $\bar{T}$ is the externally imposed uniform tension, ν is Poisson's ratio, p is the pressure, and $\bar{p}$ is the mean value of p. Also, $\delta = 0$ signifies that the downstream end is free to slide axially, whereas $\delta = 1$ if the supports do not allow net axial tension.

The above equation can be cast in nondimensional form by using following dimensionless terms:

$$\xi = x/L,\ \eta = y/L,\ \tau = \{EI/(m+\rho A)\}^{1/2}\, t/L^2. \tag{2}$$

Substitution of these terms into equation (1) yields the dimensionless equation of motion,

$$\left(\alpha\frac{\partial}{\partial\tau}+1\right)\frac{\partial^4\eta}{\partial\xi^4}+\{u^2-\delta[\Gamma+(1-2\nu)\Pi]$$
$$-\left[\frac{1}{2}\varepsilon c_T u^2+\gamma\right][(1-\frac{1}{2}\delta)-\xi]-\frac{1}{2}(1-\delta)c_b u^2\Big\}\frac{\partial^2\eta}{\partial\xi^2}$$
$$+2\beta^{1/2}u\frac{\partial^2\eta}{\partial\xi\partial\tau}+\left[\frac{1}{2}\varepsilon c_N u^2+\gamma\right]\frac{\partial\eta}{\partial\xi}$$
$$+\left[\frac{1}{2}\varepsilon c_N\beta^{1/2}u+\frac{1}{2}\varepsilon c\beta^{1/2}\right]\frac{\partial\eta}{\partial\tau}+\frac{\partial^2\eta}{\partial\tau^2}=0, \tag{3}$$

in which

$$\alpha=\left[\frac{I}{E(\rho A+m)}\right]^{1/2}\frac{E^*}{L^2},\ \beta=\frac{\rho A}{\rho A+m},\ \gamma=\frac{(m-\rho A)gL^3}{EI},$$
$$\Gamma=\frac{\bar{T}L^2}{EI},\ \varepsilon=\frac{L}{D},\ u=(\frac{\rho A}{EI})^{1/2}UL,\ \Pi=\frac{\bar{p}AL^2}{EI},$$
$$c_f=\frac{4}{\pi}C_f,\ c_N=\frac{4}{\pi}C_N,\ c_T=\frac{4}{\pi}C_T,\ c_b=\frac{4}{\pi}C_b,$$
$$c=\frac{4}{\pi}(\frac{\rho A}{EI})^{1/2}LC_D. \tag{4}$$

The boundary conditions for a cantilevered cylinder terminated by a short tapering end piece can be obtained by simplifying the equations given in Ref. [1], yielding

$$\eta(0,\tau)=\eta'(0,\tau)=0\ \text{ at }\ \xi=0, \tag{5}$$

and

$$\frac{\partial^3\eta}{\partial\xi^3}+fu^2\frac{\partial\eta}{\partial\xi}+f\beta^{1/2}u\frac{\partial\eta}{\partial\tau}-\{1+(f-1)\beta\}\chi_e\frac{\partial^2\eta}{\partial\tau^2}=0,$$
$$\frac{\partial^2\eta}{\partial\xi^2}=0\ \text{ at }\ \xi=1, \tag{6}$$

where the parameter f, which is normally less than unity, has been introduced because the theoretical lateral force at the tapered free end may not be fully realized. Also the parameter χ_e is defined as

$$\chi_e = x_e/L, \tag{7}$$

in which

$$x_e=\frac{1}{A}\int_{L-\ell}^{L}A(x)dx. \tag{8}$$

2.3 Nonlinear model

The nonlinear model for the dynamics of cantilevered cylinders in axial flow is presented in Refs. [11-13]. The equation of motion in nondimensional form is given below [12]:

$$[1+(\chi-1)\beta]\ddot{\eta}+2u\beta^{1/2}\chi\dot{\eta}'(1+\frac{7}{4}\eta'^2)+u^2\chi\eta''(1+\frac{5}{2}\eta'^2)$$
$$-\frac{3}{2}\chi\dot{\eta}\eta'(\beta\dot{\eta}'+u\beta^{1/2}\eta'')+\frac{1}{2}u^2\varepsilon c_N\left[\eta'+\frac{1}{2}\eta'^3\right]$$
$$-\frac{1}{2}u^2\varepsilon c_T(1-\xi)(\eta''+\frac{3}{2}\eta'^2\eta'')-\frac{1}{2}c_b u^2(\eta''+\eta'^2\eta'')$$
$$+(\frac{1}{2}u^2\varepsilon c_T h+\gamma)\left[\eta'+\frac{1}{2}\eta'^3-(1-\xi)(\eta''+\frac{3}{2}\eta'^2\eta'')\right]$$
$$+\eta''''+4\eta'\eta''\eta'''+\eta''^3+\eta''''\eta'^2-\frac{1}{2}\varepsilon c_N\beta\dot{\eta}\int_0^{\xi}\eta'\dot{\eta}'d\xi$$
$$+\frac{1}{2}u^2\varepsilon c_N(\frac{\beta^{1/2}}{u}\dot{\eta}-\frac{1}{2}\frac{\beta}{u^2}\dot{\eta}^2\eta'-\frac{1}{2}\frac{\beta^{1/2}}{u}\dot{\eta}\eta'^2-\frac{1}{2}\frac{\beta^{3/2}}{u^3}\dot{\eta}^3)$$
$$+\frac{1}{2}u^2\varepsilon c_d\left(\eta'|\eta'|+\frac{\beta^{1/2}}{u}(\dot{\eta}|\eta'|+\eta'|\dot{\eta}|)+\frac{\beta}{u^2}\dot{\eta}|\dot{\eta}|\right)$$
$$-\eta''(1-\beta)\int_{\xi}^{1}\int_0^{\xi}(\dot{\eta}'^2+\eta'\ddot{\eta}')d\xi d\xi$$

$$+2\chi(\beta\dot{\eta}'+u\beta^{1/2}\eta'')\int_0^{\xi}\eta'\dot{\eta}'d\xi$$

$$-\chi\eta''\int_{\xi}^{1}(\beta\ddot{\eta}\eta'+2u\beta^{1/2}\dot{\eta}'\eta'+u^2\eta''\eta')d\xi$$

$$+\eta'(1+(\chi-1)\beta)\int_0^{\xi}(\dot{\eta}'^2+\eta'\ddot{\eta}')d\xi$$

$$+\eta''\int_{\xi}^{1}\left\{\frac{1}{2}c_b u^2\eta'\eta''+\frac{1}{4}\varepsilon c_T\beta\dot{\eta}^2\right\}d\xi$$

$$+\frac{1}{2}u^2\eta''(\varepsilon c_T-\varepsilon c_N)\int_{\xi}^{1}\left(\eta'^2+\frac{\beta^{1/2}}{u}\eta'\dot{\eta}\right)d\xi+\mathrm{O}(\varepsilon^5)=0. \qquad (9)$$

where the prime and overdot stand for $\partial(\,)/\partial\xi$ and $\partial(\,)/\partial\tau$, respectively.

The following dimensionless equation represents the transverse shear boundary condition at the free end ($\xi=1$) [12]:

$$-\eta'''+\chi_e[(1+(\chi f-1)\beta)\ddot{\eta}+\chi fu\beta^{1/2}\dot{\eta}']$$
$$+(\frac{1}{2}\bar{\chi}_e\varepsilon c_N-\chi f)(u\beta^{1/2}\dot{\eta}+u^2\eta')$$
$$+(\frac{1}{2}u^2\varepsilon c_T h+\gamma)\chi_e\eta'=0, \qquad (10)$$

where the parameter χ is the virtual mass coefficient and h is the ratio of the diameter of cylinder to the hydraulic diameter. For unconfined flow, $\chi=1$ and $h=0$. Also, the parameters χ_e and $\bar{\chi}_e$ are defined by the following equation:

$$\chi_e=s_e/L,\ \bar{\chi}_e=\bar{s}_e/L, \qquad (11)$$

where

$$s_e=\frac{1}{A}\int_{L-\ell}^{L}A(s)ds,\ \bar{s}_e=\frac{1}{D}\int_{L-\ell}^{L}D(s)ds. \qquad (12)$$

The other boundary conditions including the geometrical conditions at the clamped end ($\xi=0$) and the bending moment at the free end ($\xi=1$) are the same as in the linear model, as in equations (5) and (6).

2.4 Hybrid model

The hybrid model has been developed by considering linear fluid dynamic terms while retaining a nonlinear formulation for the structural dynamics. The equation of motion in this case is given in the following equation in the dimensionless form:

$$[1+(\chi-1)\beta]\ddot{\eta}+2u\beta^{1/2}\chi\dot{\eta}'+\left\{\frac{1}{2}u\beta^{1/2}\varepsilon c_N+\frac{1}{2}\beta^{1/2}\varepsilon c\right\}\dot{\eta}$$

$$+\left\{\frac{1}{2}u^2\varepsilon c_N+(\frac{1}{2}u^2\varepsilon c_T h+\gamma)\right\}\eta'$$

$$+\left\{u^2\chi-\frac{1}{2}c_b u^2-(\frac{1}{2}u^2\varepsilon c_T+\frac{1}{2}u^2\varepsilon c_T h+\gamma)(1-\xi)\right\}\eta''$$

$$+\left(\frac{1-\beta}{1-2\beta}\right)\gamma\left[\frac{1}{2}\eta'^3-(1-\xi)\frac{3}{2}\eta'^2\eta''\right]$$

$$+\eta''''+4\eta'\eta''\eta'''+\eta''^3+\eta''''\eta'^2$$

$$-\eta''(1-\beta)\int_{\xi}^{1}\int_0^{\xi}(\dot{\eta}'^2+\eta'\ddot{\eta}')d\xi d\xi$$

$$+\eta'(1-\beta)\int_0^{\xi}(\dot{\eta}'^2+\eta'\ddot{\eta}')d\xi=0. \qquad (13)$$

The transverse shear boundary condition for this model is the same as for the nonlinear model (equation (10)) except for one extra term due to the linearized form of pressure drag within the normal frictional force; thus,

$$-\eta'''+\chi_e[(1+(\chi f-1)\beta)\ddot{\eta}+\chi fu\beta^{1/2}\dot{\eta}']$$
$$+\frac{1}{2}\bar{\chi}_e\varepsilon c\beta^{1/2}\dot{\eta}+(\frac{1}{2}\bar{\chi}_e\varepsilon c_N-\chi f)(u\beta^{1/2}\dot{\eta}+u^2\eta')$$
$$+(\frac{1}{2}u^2\varepsilon c_T h+\gamma)\chi_e\eta'=0\,. \qquad (14)$$

2.5 Method of analysis

A similar approach as in Ref. [12] is used to include the complementary end-shear boundary condition due to the tapering end in the final equation of motion, via a Dirac delta function. Then, the cantilevered beam eigenfunctions $\phi_j(\xi)$ satisfying the classical boundary conditions for a cantilevered beam are used directly as comparison functions to discretize the final equation of motion by means of Galerkin's method.

2.6 Method of solution

The discretized set of equations is solved by using a numerical scheme based on Houbolt's Finite Difference Method (FDM). It is an initial-value problem solver in which the system of equations is integrated numerically for one initial condition at a time, and the state of the system can be reproduced for any time thereafter. This scheme has been discussed in detail by Semler [23]. This method is able to predict only the stable solution branches. To obtain the unstable branches, AUTO [24], which is based on a collocation method and adapted to solving continuation and bifurcation problems for differential equations, is used. FDM together with AUTO can provide a good picture of the dynamics.

3. NUMERICAL RESULTS AND DISCUSSION

Three different sets of system parameters are used. These nondimensional parameters come from the physical parameters used in experiments reported in [1], [5] and [11] and also the nondimensional parameters used in order to validate the theoretical models proposed there. For each test case the data obtained or known from all three models (linear, nonlinear and hybrid models) are presented. In the present study, $N = 6$ modes have been used in the Galerkin approximation for all the cases. Also, $N = 8$ modes have been used in AUTO. The bifurcation diagrams obtained from nonlinear and hybrid models along with numerical comparisons are given in the subsequent parts.

3.1 Test case I

The first system is a linear system considered in Ref. [1]; the system parameters are given in Table 1.

Table 1. Nondimensional parameters of the cylinder for case I

Parameter	Value	Parameter	Value
β	0.47	χ_e	0.00667
f	0.80	$\bar{\chi}_e$	0.00785
c_b	0.20	γ	0.0
εc_f	2.50	χ	1.0

Figures 2 and 3 show the bifurcation diagrams obtained by FDM for the nonlinear and hybrid models, respectively. In addition, the bifurcation diagram obtained from the hybrid model using AUTO is given in Figure 4. In these figures the dimensionless amplitude of motion of the free end of the cylinder ($\xi = 1$) has been plotted against the dimensionless flow velocity (u). It is seen in both Figure 2 and Figure 3 that the system loses stability by static divergence through a pitchfork bifurcation at $u = u_{cd} \simeq 2.5$. The amplitude of the static deformation at $\xi = 1$ increases with u and then decreases in Figure 2, indicating that the mode shape is no longer similar to that of the first beam mode. In Figure 3, on the other hand, the amplitude at $\xi = 1$ keeps increasing. The full nonlinear model of Figure 2 predicts a Hopf bifurcation at $u \simeq 7.6$, indicating the onset of flutter. This bifurcation emerges from a non-trivial solution, and it is not captured by the hybrid model, as seen in Figures 3 and 4. However, as seen in Figure 4, AUTO detects a second pitchfork bifurcation at $u \simeq 7.7$ for the hybrid model, leading to an unstable solution branch.

The numerical results are given in Table 2. In the table, u_{cd} represents the critical velocity for divergence, while u_{cf} is the critical velocity for flutter. The reason for the hybrid model not predicting the coupled-mode flutter at $u_{cf} = 7.68$ found by the linear model, predicting a second divergence instead at $u \simeq 7.7$ is not clear.

However, the main drawback of the hybrid model whether by means of FDM or AUTO is that it gives non-physical amplitudes, i.e. amplitudes larger than the cylinder length. The full nonlinear model, on the other hand, predicts physically more reasonable maximum amplitudes, of the order of 20% of the length.

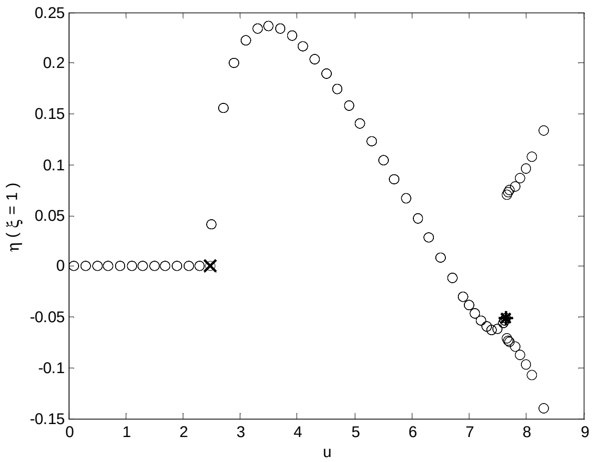

Figure 2. Bifurcation diagram obtained with nonlinear model using FDM for case I: $\times$ shows the onset of divergence; $*$ shows the onset of flutter

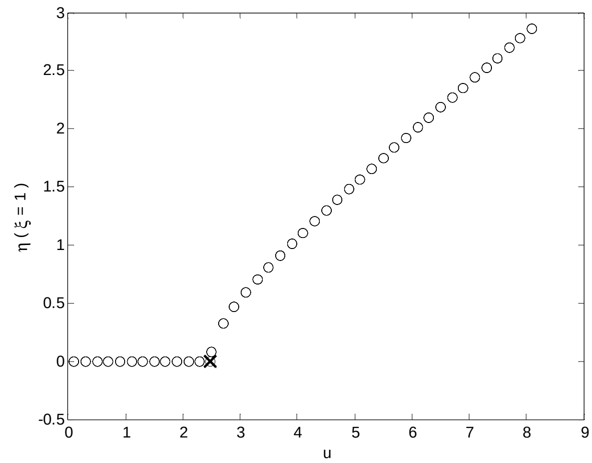

Figure 3. Bifurcation diagram obtained with hybrid model using FDM for case I: $\times$ shows the onset of divergence

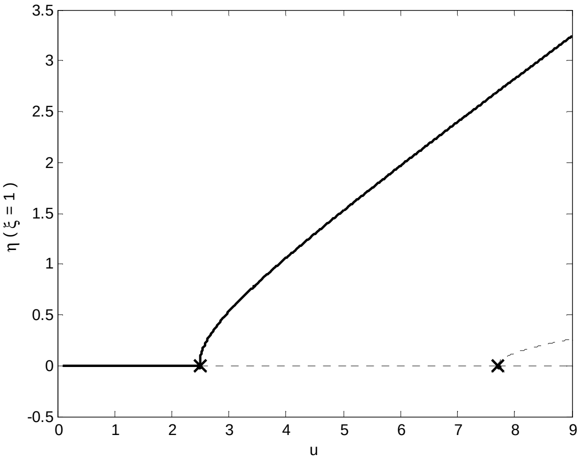

Figure 4. Bifurcation diagram obtained with hybrid model using AUTO for case I: continuous line, stable solutions; dashed line, unstable solutions; $\times$ shows the onset of divergence

Table 2. The onset of different instabilities predicted by different models for case I

Analytical model used	u_{cd}	u_{cf}
Linear [1]	2.49	7.68§
Nonlinear	2.47 [2.49]	7.64 [7.64]
Hybrid	2.47 [2.49]	--- [---]

§ : this value has been obtained from a more accurate analysis (with a high number of Galerkin modes) with respect to Ref. [1]
[ ] : gives the numerical values obtained by means of AUTO
--- : signifies that the phenomenon could not be captured

The numerical values presented in Table 2 show very good agreement between the different models (from linear to nonlinear and hybrid models) in predicting the onset of first instability, as it should be. Also, the numerical values found by FDM are confirmed by the numerical values given by AUTO.

3.2 Test case II

The system parameters for this case study are tabulated in Table 3. Again, a linear analysis of the system has been performed by Païdoussis [5].

Table 3. Nondimensional parameters of the cylinder for case II

Parameter	Value	Parameter	Value
β	0.20	χ_e	0.02
f	0.80	$\bar{\chi}_e$	0.00
c_b	0.10	γ	0.0
εc_f	0.20	χ	1.0

Figures 5 and 6 show the bifurcation diagram obtained from the nonlinear and hybrid models, respectively, and Figure 7 presents the bifurcation diagram obtained with the hybrid model using AUTO. Again, in these figures the nondimensional amplitude at the free end of the cantilevered cylinder was plotted versus the nondimensional flow velocity. The onsets of divergence and flutter based on the linear model could be obtained by using the graphs provided in Ref. [5, Fig. 8]. But, in the course of this work, it has been found that they are insufficiently accurate; therefore, a more accurate linear analysis (with a high number of Galerkin modes) has been done to find the onset of divergence and flutter. All the numerical values for the critical flow velocities obtained by the different models are summarized in Table 4.

As seen from Figure 5, the nonlinear model using FDM cannot predict a post-divergence flutter. This can only be concluded when a high number of Galerkin modes, e.g. $N = 10$ is used in FDM. On the other hand, the hybrid model shows a different behaviour: as seen in Figure 6, FDM could not find any post-divergence instability, but AUTO is successful, predicting an unstable Hopf bifurcation at $u = 3.88$. The reason why FDM cannot find the Hopf bifurcation for both fully nonlinear and hybrid models, is due to the inherent inability of FDM to find unstable solutions.

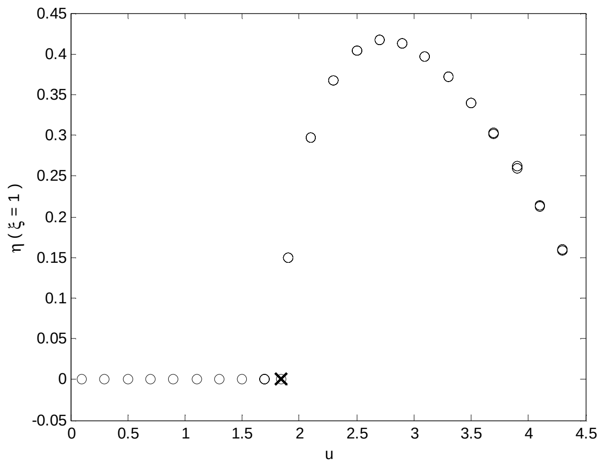

Figure 5. Bifurcation diagram obtained with nonlinear model using FDM for case II: $\times$ shows the onset of divergence

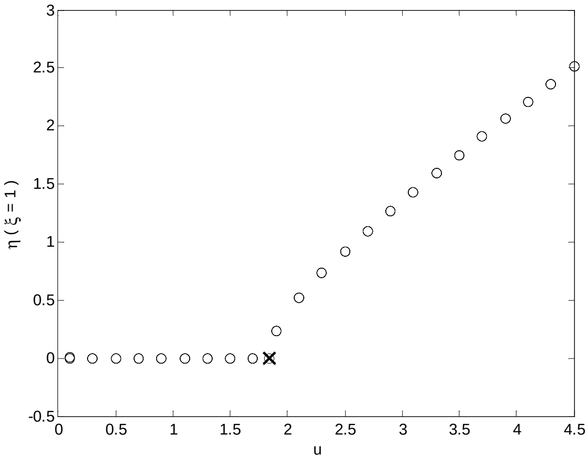

Figure 6. Bifurcation diagram obtained with hybrid model using FDM for case II: × shows the onset of divergence

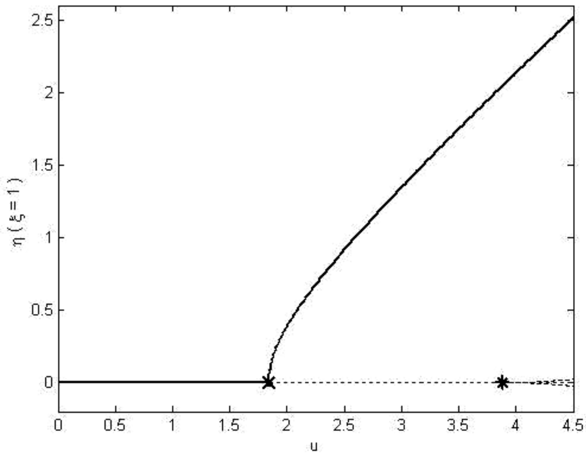

Figure 7. Bifurcation diagram obtained with hybrid model using AUTO for case II: continuous line, stable solutions; dashed line, unstable solutions; × shows the onset of divergence, and ∗ shows the onset of flutter

Table 4. The onset of different instabilities predicted by different models for case II

Analytical model used	u_{cd}	u_{cf}
Linear §	1.84	3.88
Nonlinear	1.84 [1.84]	--- [3.88]
Hybrid	1.84 [1.84]	--- [3.88]

§ : these values have been obtained from a more accurate analysis (with a high number of Galerkin modes) with respect to Ref. [5]

[ ] : gives the numerical values obtained by means of AUTO

--- : signifies that the phenomenon could not be captured

3.3 Test case III

The parameter set for this test case is similar to the first set except for the dimensionless parameter of gravity, which is not zero, and a lower friction coefficient. The numerical values of the parameters are given in Table 5.

Table 5. Nondimensional parameters of the cylinder for case III

Parameter	Value	Parameter	Value
β	0.47	χ_e	0.00667
f	0.70	$\bar{\chi}_e$	0.00785
c_b	0.30	γ	1.9
εc_f	0.50	χ	1.0

The bifurcation diagram for this system obtained with the nonlinear model is given in Figure 8. From that diagram the onset of two instabilities can be identified. The corresponding instabilities have also been obtained with the linear and hybrid models. Figure 9 shows the bifurcation diagram obtained via the hybrid model by means of FDM, and Figure 10 presents the bifurcation diagram obtained with the hybrid model using AUTO.

Table 6 makes a numerical comparison between the onsets of different possible instabilities predicted by the three models.

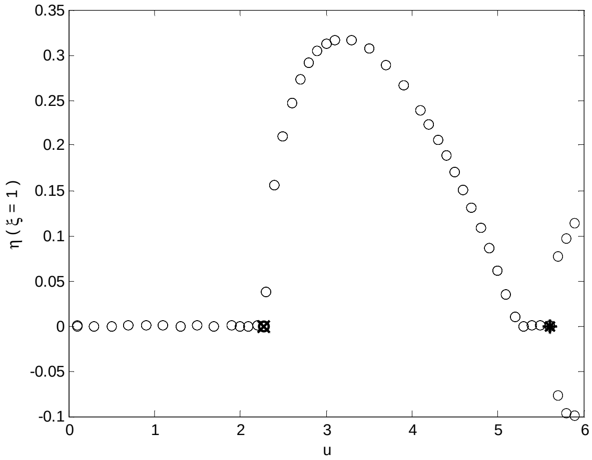

Figure 8. Bifurcation diagram obtained with nonlinear model using FDM for case III: × shows the onset of divergence; ∗ shows the onset of flutter

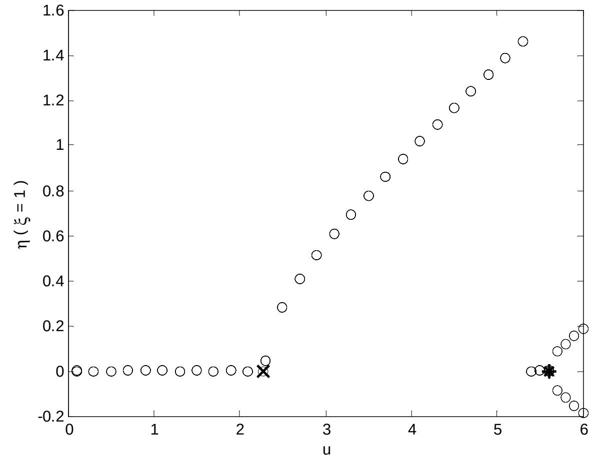

Figure 9. Bifurcation diagram obtained with hybrid model using FDM for case III: × shows the onset of divergence; * shows the onset of flutter

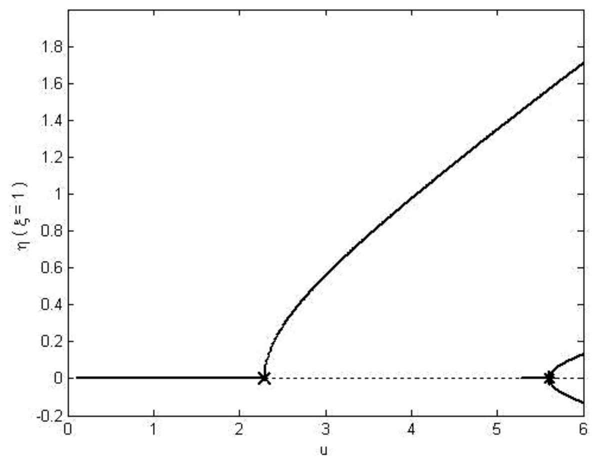

Figure 10. Bifurcation diagram obtained with hybrid model using AUTO for case III: continuous line, stable solutions; dashed line, unstable solutions; × shows the onset of divergence, and * shows the onset of flutter

Table 6. The onset of different instabilities predicted by different models for case III

Analytical model used	u_{cd}	u_{cf}
Linear	2.29	5.61
Nonlinear	2.28 [2.29]	5.60 [5.60]
Hybrid	2.28 [2.29]	5.60 [5.60]

[ ] : gives the numerical values obtained by means of AUTO

As seen from Figures 8 to 10 and according to the numerical comparison given in Table 6, the hybrid model can predict the onset of the first and second instabilities with both FDM and AUTO, with a very good agreement with respect to the nonlinear model. Here, the post-divergence instability emerges from the trivial equilibrium state of the system, and it leads to a stable solution branch and that is why it could be captured even by FDM. However, the main disadvantage to the hybrid model, namely that it predicts unreasonably large amplitudes, still exists and seems to be inherent in this model.

3.4 Discussion

According to the bifurcation diagrams depicted in the Figures 2-10 and according to the numerical comparisons provided in Tables 2, 4 and 6, it is shown that the hybrid model gives non-physical amplitudes. Moreover, it is not even able to predict the whole qualitative picture of the dynamics in all cases; although in case III it does. Nevertheless, the hybrid model is capable of predicting the onset of instabilities which emerge from the trivial equilibrium state, but it cannot give numerical values with a better correlation to the nonlinear results relative to the linear model.

Also, it is found that FDM solutions for the hybrid model are even less successful than those obtained by AUTO, because only stable trivial solutions can be captured and, therefore, they cannot predict the post-divergence instability in many cases.

4. CONCLUSION

In this paper a hybrid model, using linear fluid dynamics while retaining nonlinear structural dynamics in the equations of motion, has been presented. The capabilities of this model in predicting the dynamical behaviour of cantilevered cylinders in axial flow, such as the onset of instabilities, have been tested. In addition, the linear and fully nonlinear models have also been utilized in the paper, to compare with the hybrid model. Some numerical results alongside some graphical results have also been presented for comparison. The expectation that the hybrid model could offer significant improvements relative to the linear model while having a simpler form relative to the nonlinear model have turned out to be wrong. Therefore, it is clear that the 3-D model which needs to be developed must be a fully nonlinear one.

5. ACKNOWLEDGMENTS

The support to this research by NSERC of Canada is gratefully acknowledged. The first author also greatly appreciates Ms. Anahita Mansouri Bigvand support during his Ph.D. studies.

REFERENCES

1. Païdoussis, M.P., *Fluid-Structure Interactions : Slender Structures and Axial Flow*. 2004. London: Elsevier Academic Press.
2. Hawthorne, W.R. The early development of the Dracone flexible barge. In *Proceedings of the Institution of Mechanical Engineers*, 1961, **175**: 52-83.

3. Païdoussis, M.P., Dynamics of flexible slender cylinders in axial flow. Part 1. Theory. *Journal of Fluid Mechanics*, 1966, **26**: 717-736.
4. Païdoussis, M.P., Dynamics of flexible slender cylinders in axial flow. Part 2. Experiments. *Journal of Fluid Mechanics*, 1966, **26**: 737-752.
5. Païdoussis, M.P., Dynamics of cylindrical structures subjected to axial flow. *Journal of Sound and Vibration*, 1973, **29**(3): 365-385.
6. Païdoussis, M.P., Dynamical behavior of cylindrical structures in axial flow. *Annals of Nuclear Science and Engineering*, 1974, **1**(2): 83-106.
7. Ortloff, C.R. and J. Ives, On the dynamic motion of a thin flexible cylinder in a viscous stream. *Journal of Fluid Mechanics*, 1969, **38**: 713-720.
8. Pao, H.P. and Q. Tran, Response of a towed thin flexible cylinder in a viscous fluid. *Journal of the Acoustical Society of America*, 1973, **53**(5): 1441-1444.
9. Triantafyllou, G.S. and C. Chryssostomidis, Analytic determination of the buckling speed of towed slender cylindrical beams. *ASME Journal of Energy Resources Technology*, 1984, **106**(2): 246-249.
10. Triantafyllou, G.S. and C. Chryssostomidis, Stability of a string in axial flow. *ASME Journal of Energy Resources Technology*, 1985, **107**(4): 421-425.
11. Païdoussis, M.P., E. Grinevich, D. Adamovic, and C. Semler, Linear and nonlinear dynamics of cantilevered cylinders in axial flow. Part 1: Physical dynamics. *Journal of Fluids and Structures*, 2002, **16**(6): 691-713.
12. Lopes, J.-L., M.P. Païdoussis, and C. Semler, Linear and nonlinear dynamics of cantilevered cylinders in axial flow. Part 2: The equations of motion. *Journal of Fluids and Structures*, 2002, **16**(6): 715-737.
13. Semler, C., J.-L. Lopes, N. Augu, and M.P. Païdoussis, Linear and nonlinear dynamics of cantilevered cylinders in axial flow. Part 3: Nonlinear dynamics. *Journal of Fluids and Structures*, 2002, **16**(6): 739-759.
14. Modarres-Sadeghi, Y., M.P. Païdoussis, and C. Semler, A nonlinear model for an extensible slender flexible cylinder subjected to axial flow. *Journal of Fluids and Structures*, 2005, **21**: 609-627.
15. Modarres-Sadeghi, Y., M.P. Païdoussis, and C. Semler, The nonlinear behaviour of a slender flexible cylinder pinned or clamped at both ends and subjected to axial flow. *Computers & Structures*, 2007, **85**: 1121-1133.
16. Païdoussis, M.P., Stability of towed totally submerged flexible cylinders. *Journal of Fluid Mechanics*, 1968, **34**: 273-297.
17. Païdoussis, M.P., Dynamics of submerged towed cylinders. M.E.R.L. T.N. 70-4, 1970, Montreal: McGill University.
18. Païdoussis, M.P. and B.K. Yu, Elastohydrodynamics and stability of towed slender bodies of revolution. *Journal of Hydronautics*, 1976, **10**: 127-134.
19. Dowling, A.P., The dynamics of towed flexible cylinders. Part 1: Neutrally buoyant elements. *Journal of Fluid Mechanics*, 1988, **187**: 507-532.
20. Dowling, A.P., The dynamics of towed flexible cylinders. Part 2: Negatively buoyant elements. *Journal of Fluid Mechanics*, 1988, **187**: 533-571.
21. Wang, L. and Q. Ni, Vibration of slender structures subjected to axial flow or axially towed in quiescent fluid. *Advances in Acoustics and Vibration*, 2009, Article ID 432340: 19 pages.
22. Amabili, M., F. Pellicano, and M.P. Païdoussis, Non-linear dynamics and stability of circular cylindrical shells containing flowing fluid. Part I: Stability. *Journal of Sound and Vibration*, 1999, **225**(4): 655-699.
23. Semler, C. and M.P. Païdoussis, Nonlinear analysis of the parametric resonances of a planar fluid-conveying cantilevered pipe. *Journal of Fluids and Structures*, 1996, **10**(7): 787-825.
24. Doedel, E.J. and J.P. Kerneves, AUTO: software for continuation and bifurcation problems in ordinary differential equations. Applied Mathematics Report, 1986: California Institute of Technology, Pasadana, CA, USA.